https://dx.doi.org/10.1016/j.combustflame.2022.112344

Unraveling the role of EGR olefins at advanced combustion conditions in the presence of nitric oxide: ethylene, propene and iso-butene

Song Cheng[a,b,d,*], Chiara Saggese[c,*], S. Scott Goldsborough[a,*], Scott W. Wagnon [c], William J. Pitz[c]

[a] *Energy Systems Division, Argonne National Laboratory, Lemont, IL 60439, USA*

[b] *Department of Mechanical Engineering, The Hong Kong Polytechnic University, Kowloon, Hong Kong*

[c] *Materials Science Division, Lawrence Livermore National Laboratory, Livermore, CA 94551, USA*

[d] *Research Centre for Resources Engineering towards Carbon Neutrality, The Hong Kong Polytechnic University, Kowloon, Hong Kong*

*Corresponding authors:

Song Cheng
Email: songcheng@polyu.edu.hk

Chiara Saggese
Email: saggese1@llnl.gov

S Scott Goldsborough
Email: sgoldsborough@anl.gov

Abstract

The role of EGR (exhaust gas recirculation) olefinic constituents at advanced combustion conditions in the presence of nitric oxide is unraveled in this study through experimental and modeling efforts using a twin-piston rapid compression machine operating at a stochiometric fuel loading with 20% EGR by mass, pressures of 20 and 40 bar, and temperatures from 680 to 950 K. Five different levels of olefin addition, focusing on ethylene, propene and iso-butene, with a fixed amount of NO at 70 ppm are doped into test mixtures of PACE-20, a multi-component gasoline surrogate, where olefin addition effects are characterized through changes in ignition times and heat release rates. Experiments indicate that all three EGR olefins inhibit autoignition reactivity and low-temperature heat release at Tc < 850 K, with iso-butene exhibiting the greatest impact, while at Tc >850 K, low ethylene and propene additions promote reactivity. A recently updated chemical kinetic model, with detailed gasoline/NO_x interacting and olefin/NO_x interacting chemistry incorporated, is adopted to simulate the experiments. Simulation results are somewhat inconsistent with the experiments, where the model captures the inhibiting effects of all olefins on first-stage ignition reactivity, while consistently predicting a promoting effect on main ignition reactivity. Sensitivity and rate of production analyses reveal that adding olefins greatly alters the role of the consuming pathways for the olefins and their primary derivatives at the initial stage of the oxidation process, particularly with the presence of NO, where the olefins and their derivatives interact with both NO_x species such as NO_2 and other species such as OH and HO_2. The olefin/NO_x interactions are particularly pronounced with propene and iso-butene addition, where these lead to increased ignition reactivity by facilitating NO production and are mostly responsible for the disagreement between the model and experiments. Further investigations of olefin interacting chemistry, particularly those with NO_x species, are needed for chemistry models to accurately predict the complicated effects of EGR.

Keywords: EGR olefins; gasoline/olefin interaction; olefin/NO_x interaction; autoignition

1. Introduction

Exhaust gas recirculation (EGR) has a long history in application to advanced internal combustion engines, providing a way to mitigate knock in spark-ignition engines [1] and control combustion phasing/heat release rates (HRRs) in homogeneous charge compression ignition engines [2], thus achieving higher engine thermal efficiency, higher fuel economy and lower emissions. Introducing EGR into the engine intake imposes both physical and chemical effects. Physically, EGR dilutes the energy density and increases the heat capacity of the in-cylinder charge, yielding lower compressed and burned gas temperature/pressure. Chemically, major EGR species such as CO_2 and H_2O, and importantly, minor EGR species such as unburned hydrocarbons and NO_x can alter equilibrium and rate of elementary reactions, leading to changes in intermediate/radical pools.

Influences of EGR on gasoline combustion have been extensively characterized in both practical engines [3-7] and fundamental reactors [8-12]. However, most previous studies have focused on major EGR species. Though fairly thorough understanding has been established, gaps in physical/chemical effects of some major EGR species still exist, e.g., modeling of rapid compression machine (RCM) experiments with the presence of CO_2 has been found to inadequately replicate the high-temperature heat release process [13, 14].

In contrast to the major EGR species, influences of minor EGR species have received relatively less attention in the past. Many of these efforts have emphasized gasoline/NO_x chemical kinetic interactions, e.g., [12, 15], with very few focusing on other trace EGR species such as olefins, though their importance has been highlighted in a few studies. For instance, Szybist [16] detected ethylene as the most dominant EGR olefins (on the order of 100–200 ppm) in a modified gasoline engine and found that untreated EGR that contains ethylene was less effective at mitigating knock compared to treated EGR. Kobashi et al. [17] detected ~1000 ppm of ethylene, as well as large amount of propene and iso-butene in the air intake of a modified diesel engine. By seeding both NO and olefins into the engine intake, they found that ethylene and propene demonstrate a negligible effect without NO and a strong promoting effect with NO on engine autoignition. These studies indicate that EGR olefins can interact with both fuel derivatives and EGR NO_x species, imposing complicated impacts on engine combustion characteristics.

Despite their importance, fundamental studies investigating EGR olefin/gasoline interactions have been seriously lacking, let alone those with the presence of NO. To date, ethylene autoignition has only been investigated in an RCM as a component of an ethylene-nitrous oxide propellent [18]; propene autoignition has only been investigated individually and as a component of a propane/propene mixture in another RCM [19]; and iso-butene autoignition has only been investigated in [20].

Therefore, this study aims to: (a) understand the chemical kinetic interactions between EGR olefins and major species derived from gasoline fuels, and those between EGR olefins and NO_x species; (b) investigate the perturbative effects of these interactions on gasoline autoignition and heat release characteristics; and (c) provide experimental data to properly formulate high-fidelity chemical kinetic models. To this end, new measurements are conducted for a gasoline surrogate in an RCM with 20% EGR by mass, 70 ppm NO and different olefin additions at pressures of 20 and 40 bar, and temperatures from 700 to 930 K. Three olefins are investigated, namely ethylene (C_2H_4), propene (C_3H_6) and iso-butene (iC_4H_8), where changes in ignition reactivity and heat release behavior are quantified and compared across different levels of olefin addition. A recently updated gasoline surrogate model, with specific gasoline/NO_x interactions and olefin/NO_x interactions incorporated, is used to model the RCM experiments and generate further insight into the olefin addition effects.

2. Experimental and computational methods

2.1 Gasoline surrogate

PACE-20 is a high-fidelity, multi-component gasoline surrogate developed for a research-grade, US E10 (10% liquid volume ethanol) gasoline, termed RD5-87. It is formulated targeting a comprehensive set of physical and chemical properties of RD5-87 by a working group of the PACE consortium, with superior performance in replicating RD5-87 compared to other surrogates. Details of the surrogate formulation and its performance have been well documented in [21], hence will not be discussed here. The composition and selected properties of PACE-20 and RD5-87 are summarized in Table 1.

Table 1
Percent composition (liquid volume basis) and selected properties of RD5-87 and PACE-20.

	RD5-87	**PACE-20**

n-**P**araffins	16.8	*n*-Pentane	14.0
		n-Heptane	11.5
***I**so*-paraffins	32.8	*Iso*-octane	25.0
Olefins	6.7	1-Hexene	5.4
Naphthenes	11.5	Cyclopentane	10.5
Aromatics	22.1	Toluene	9.2
		1,2,4-Trimethylbenzene	11.9
		Tetralin	3.0
o**X**ygenates	10.1	Ethanol	9.6
RON	92.3	92.1	
MON	84.6	84.5	
AKI	88.4	88.3	

2.2 Experimental

2.2.1 RCM description

A heated twin-piston RCM (tpRCM) at Argonne National Laboratory (ANL) is utilized for this study. A detailed description of its configuration and recent modifications, as well as uncertainties associated with measurements can be found in [22, 23], and are briefly described here. A single compression event is driven by a pneumatic system, with a hydraulic ring-groove system used at the end of the stroke to arrest the fast-moving pistons and lock them in place. The reaction chamber pistons utilize crevices machined around their circumference [22] to suppress possible roll-up vortices during the compression, thus improving post-compression charge homogeneity. Electrical-heating tapes are used to heat the reaction chamber to desired temperature, with high-density insulation used to isolate it from the hydraulic chamber. Dynamic pressure is measured using an uncoated, diaphragm-reinforced, thermal-shock resistant Kistler 6045A-U20 pressure transducer calibrated to 250 bar and coupled to a Kistler 5064 charge amplifier.

2.2.2 EGR mixing (excluding NO and olefin)

The EGR used in this study is assumed to consist of complete combustion products (N_2, CO_2 and H_2O) at the stoichiometry of 1.0 for PACE-20, which is prepared and premixed with the PACE-20/oxidizer mixture in a 5.6 L, stainless steel tank, heated to 70 °C, prior to the experiments. CO is not considered in this study as its concentration in EGR is quite low at diluted/stoichiometric conditions [24], and its chemical impact on fuel autoignition reactivity is negligible at low to intermediate temperatures [25]. PACE-20 is first introduced into the purged and evacuated tank

using a weighed syringe, and the high purity gases are then supplied to the tank in the sequence of Ar (99.9997%, Airgas), N2 (99.9998%, Airgas) and O_2 (99.9997%, Airgas). Thereafter, liquid H_2O (99.99%) is injected into the mixing tank using another weighed syringe. Then the PACE-20/oxidizer/EGR mixture is isolated for at least 4 hours to diffusively homogenize. The partial pressure of H_2O in the mixture is maintained at <50% of its saturated vapor pressure to ensure no condensation of water during the experiments. Total water evaporation, determined based on the measured water partial pressure and injected water mass, is above 90% for all the experiments.

2.2.3 Olefin mixing

In this study, olefin (ethylene (99.99% Sigma-Aldrich), propene (99.99% Sigma-Aldrich) and iso-butene (99.99%, Sigma-Aldrich)) is first premixed with N_2 (99.9998%, Airgas) in a Sigma-Aldrich Sure-Pac container. The diluted, premixed olefin/N_2 mixture is then filled into the heated mixing tank to the desired pressure after the PACE-20/oxidizer/EGR mixture (Section 2.2.2). Thereafter, the mixing tank is isolated for 1 hour. The uncertainty of olefin in the final test mixture is under ±5%, which is estimated using the linear uncertainty propagation rule with considering both the instrumental and human reading uncertainty in initial reaction chamber pressure (±(0.25% of 400–1110 + 1.0) Torr), initial filling pressure of NO/N_2 mixture in the reaction chamber and olefin/N_2 mixture in the mixing tank (±(0.25% of 20–150 + 1.0) and ±(0.25% of 100–800 + 1.0) Torr, respectively), NO mole fraction in the NO/N_2 mixture (±2 ppm), initial olefin mole fraction in the olefin/N2 mixture (overestimated at ±1%), and initial reaction chamber temperature and mixing tank temperature (±2.2 K). The uncertainty analysis results are presented in Fig. S1 in the Supplementary Material.

2.2.4 NO mixing

The test mixture containing NO is prepared in the heated reaction chamber (303–358 K) by feeding the desired amount of NO (supplied with a custom-made N_2 balanced NO cylinder from Airgas with a NO concentration of 2007±2 ppm) and PACE-20/oxidizer/EGR/olefin mixture (supplied from the mixing tank) into the reaction chamber. Prior to each NO addition experiment, the NO/N_2 mixture is first filled into the reaction chamber and isolated for 4 minutes. Thereafter, the PACE-20/oxidizer/EGR/olefin mixture is filled into the reaction chamber and isolated for 1

minute. Waiting time from 1–4 minutes for both the NO/N_2 mixture and PACE-20/oxidizer/EGR/olefin mixture has been evaluated, with no noticeable variation in ignition delay time observed. Kinetic modeling has already been conducted in [15], which indicated that at the conditions studied in this work, NO will not be noticeably concerted to NO_2 within 1 minute of contact time with O_2. The uncertainty of NO mole fraction in the test mixture is also estimated to be under ±5% using the linear uncertainty propagation method described in Section 2.2.3.

2.2.5 Data analysis

The compressed temperature (Tc), main ignition delay time (τ) and heat release rates (HRR) are determined by post-processing recorded pressure traces. To ascertain the end of compression (t_0) and the extent of the heat loss during ignition delay period, a non-reactive test, wherein O_2 in the test mixture is replaced with N_2, is conducted for each reactive condition. Tc is calculated using adiabatic core hypothesis: $\int_{T_i}^{T_c} \frac{\gamma}{\gamma-1}\frac{dT}{T} = \frac{\ln P_c}{P_i}$, where subscripts '$i$' and '$c$' indicate the initial and compressed conditions, and γ is the ratio of specific heats of the mixture.

An energy balance approach [26] is used to calculate the HRR, and accumulated, or integrated heat release. This can be expressed as,

$$HRR = \frac{\gamma}{\gamma-1}\frac{dV}{dt}[P - P_{nr}] + \frac{1}{\gamma-1}V\left[\frac{dP}{dt} - \left.\frac{dP}{dt}\right|_{nr}\right] - \frac{PV}{(\gamma-1)^2}\left[\frac{d\gamma}{dt} - \left.\frac{d\gamma}{dt}\right|_{nr}\right] \quad (1)$$

where the subscript 'nr' indicates non-reacting condition. The gas temperature during the reactive tests is calculated as, $T \approx T_{nr} + x_b(LHV_{mix}/c_v)$, where LHV_{mix} is the lower heating value of the mixture, c_v is the constant-volume specific heat of the mixture, and x_b is the fraction of fuel energy released, which is deduced from $\int(HRR)dt/LHV_{mix}$.

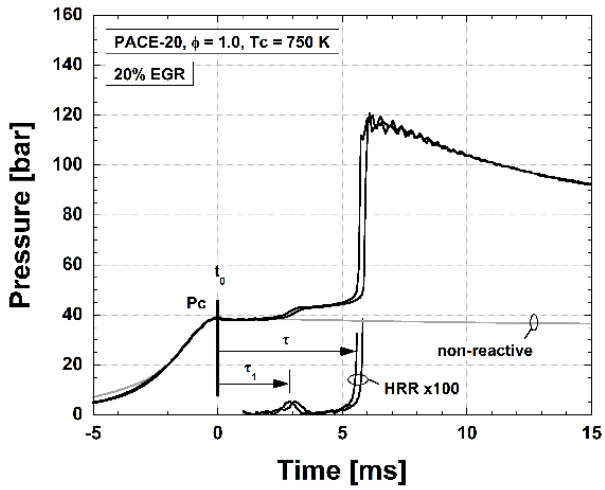

Figure 1. Representative reactive and non-reactive pressure-time histories for PACE-20 at ϕ = 1.0, Pc = 40 bar and Tc = 750 K, with 20% EGR by mass and without olefin and NO doping. The normalized HRR trajectory is also presented.

Representative reactive and non-reactive pressure-time histories for PACE-20 with 20% EGR by mass and without NO and olefin addition at Tc = 720 K and Pc = 40 bar are presented in Fig. 1, where first-stage and main ignition delay times are defined. At least two tests are conducted at each condition to ensure good repeatability. The corresponding HRR trajectory is also included in Fig. 1, where low-temperature heat release (LTHR) and intermediate-temperature heat release (ITHR), are determined [27]. An uncertainty analysis associated with ANL's tpRCM is documented in [22], leading to ±1.5%, ±15% and ±10% in conservative estimates to Tc, τ and HRR, respectively. Specifically, uncertainty of Tc is estimated also using linear propagation considering the uncertainties in Ti, Pi, Pc and γ, following [28]; that of τ is estimated from data scatter over months, i.e., standard deviation of repeated measurements. It should be noted that determining the full uncertainty in τ requires utilizing comprehensive uncertainty analysis frameworks, such as [29], which is beyond the scope of this work.

2.2.6 Test mixtures

A diluted/stoichiometric operating condition (15.7% O_2, ϕ = 1.0) is considered in this work, with 20% EGR (mass basis) and 70 ppm NO employed, and two different diluents, Ar and N_2, utilized to cover the desired Tc range (680–950 K). Five olefin additions are studied, including 0, 100, 200, 800 and 3200 ppm. 70 ppm NO was used to represent boosted SI engine combustion with

~20% EGR. The olefin concentrations were selected to cover the typical olefin concentrations in practical EGR combustion, as reported in [16, 17], with the highest value representing an extreme condition to clarify trends. Also important to note is that the olefin concentrations selected in this study should be sufficient to quantify trends with minimizing uncertainty, as have been done considerably in the past in fuel blending studies, rather than match exactly those experienced in practical engines, so that the dataset can be confidently used for model validation. The test conditions are summarized in Table 2.

Table 2
Summary of test conditions used in this study (gases are presented in mole fraction; NO and olefins presented in ppm).

Mix #	ϕ	PACE -20	O_2	N_2	Ar	CO_2	H_2O	NO /ppm	Olefins /ppm	Tc /K	Pc /bar
1	1.0	0.0187	0.1573	0.7715	0	0.0272	0.0247	70	0–3200	<800	20, 40
2	1.0	0.0187	0.1573	0.2769	0.4946	0.0272	0.0247	70	0–3200	>800	20, 40

2.3 Modeling

The kinetic model developed in the work of Cheng et al. [13] combined with the NO_x chemistry developed in Fang et al. [15] is adopted in this study. Regarding NO_x/hydrocarbons interacting chemistry, new reactions are added for several PACE-20 components, namely ethanol, 1-hexene, 1,2,4-trimethylbenzene and cyclopentane, and for other aromatics, such as benzene, o-xylene and p-xylene, following the reaction classes and related kinetic parameters presented in Fang et al. [15] and as summarized in Table 3. The updated chemical kinetic model and its validation against ignition delay time and heat release experiments for PACE-20/NO mixtures can be found in [30].

Table 3. Newly added NO_x reaction classes.

Index	Reaction Class	$k = AT^n \exp(-E/RT)$[a]			Reference
		A	n	E	
1	$RH + NO_2 \Leftrightarrow \dot{R} + HONO$	Primary H: 2.2×10^{13}	0	31.1	[31]
		Secondary H: 5.8×10^{12}	0	28.1	
		Tertiary H: 9.3×10^{12}	0	25.8	
2	$R + HNO \Leftrightarrow NO + RH$	1.47×10^{11}	0.76	0.349	CH_3+HNO=NO+CH_4 [32]
3[b]	$\dot{R} + NO_2 \Leftrightarrow R\dot{O} + NO$	1.1×10^{13}	0	0	$\dot{C}H_3$+NO_2=NO+$CH_3\dot{O}$ [33]
3[c]	$\dot{R} + NO_2 \Leftrightarrow R\dot{O} + NO$	0.6×10^{13}	0	0	$\dot{C}_3H_5$+NO_2=NO+$C_3H_5\dot{O}$ [34, 35]
3[d]	$\dot{R} + NO_2 \Leftrightarrow RONO$ (hpl)	16.98×10^{51}	–12.45	11.72	C_7H_{15}-3+NO_2=$C_7H_{15}ONO$-3 [36]

	$RONO \Leftrightarrow R\dot{O} + NO$ (hpl)	7.31×10^{50}	–11.04	51.31	$C_7H_{15}ONO\text{-}3=C_7H_{15}\text{-}3O + NO$ [36]
	$R + NO_2 \Leftrightarrow RO + NO$ (hpl)	4.83×10^{49}	–11.34	19.48	$C_7H_{15}\text{-}3+NO_2=C_7H_{15}\text{-}3O+NO$ [36]
4	$RO\dot{O} + NO \Leftrightarrow R\dot{O} + NO_2$	1.4×10^{12}	0	-0.715	$CH_3\dot{O}_2+NO=CH_3\dot{O}+NO_2$ [37]

[a] Units are mol, cm^3, s, K, and kcal. Reaction rates for reaction class 1 are per H atom (i.e., multiply by three for one methyl group). "hpl" stands for high pressure limit.
[b] For C1–C4 alkanes, ethanol, cyclopentane, benzene and 1-hexene.
[c] For propene and iso-butene.
[d] For n-pentane, iso-pentane, n-heptane, iso-octane, toluene, 1,2,4-trimethylbenzene, p-xylene, o-xylene.

It is worth mentioning that the kinetics used for toluene/NO_x interactions published in Fang et al. [15] is further validated against ignition delay time experiments of toluene at 12% O_2, ϕ = 1.0, and 25 and 45 bar with addition of 0-200 ppm of NO (results are included in a forthcoming paper that's currently under preparation). Reactions between NO_x and olefins, such as propene and iso-butene, were added following the reaction classes in Fang et al. [15]. For propene and iso-butene, the kinetics of the reactions between the fuel radical and NO_2 is in line with recent literature studies [34, 35]. Simulations of the RCM experiments are conducted using the LLNL-developed fast-solver Zero-RK [38], using volume-time histories derived from non-reactive tests in order to account for compression and heat loss effects.

3. Results and discussion

3.1 Ignition and HRR results

PACE-20, with four different levels of olefin addition (100 (only for ethylene), 200, 800 and 3200 ppm) are tested in the ANL tpRCM at two isobaric conditions (i.e., Pc = 20 and 40 bar), ϕ = 1.0 and compressed temperatures from 680 to 950 K. Two baseline cases are also included, namely the case without olefins and NO and the case with 70 ppm NO and no olefins, for better comparison. It should be noted that at least two tests were conducted at each condition, with great consistency observed. It is also important to recognize that the objective of this study is to investigate the influences of EGR olefins on gasoline autoignition characteristics under conditions representative of boosted SI engine operation. Since NO is always present in the EGR, the olefin addition experiments were conducted with base NO addition (i.e., 70 ppm). On the other hand, it has been reported that EGR olefins have negligible influence without the presence of NO [17]. As such, experiments with only olefin addition were not performed. The measured ignition delay times and volume-time histories derived from non-reactive tests are included as Supplementary Materials.

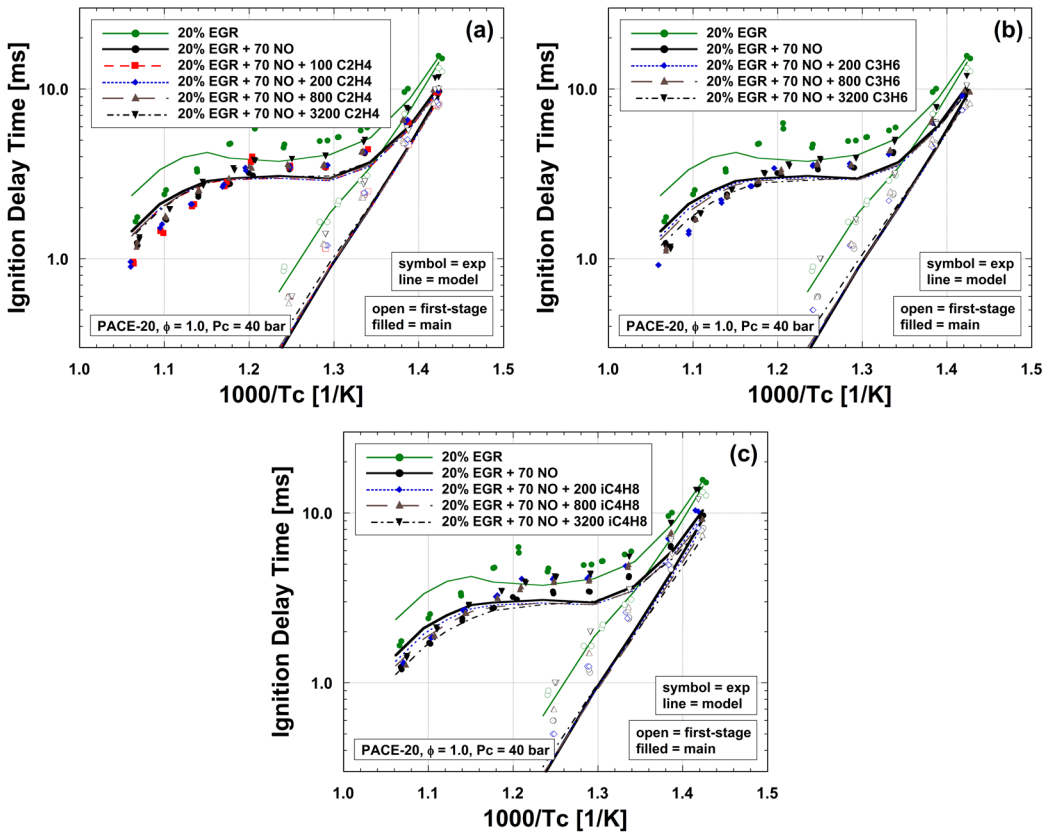

Figure 2. Measured (symbols) and simulated (lines) ignition delay times presented as functions of inverse temperature for PACE-20 with 20% EGR by mass, 70 ppm NO and different olefin concentrations (0, 100, 200, 800 and 3200 ppm) at **Pc = 40 bar**: (a) ethylene (C_2H_4); (b) propene (C_3H_6); (c) iso-butene (iC_4H_8). Lines – simulation results; symbols – experiments. 20% EGR + 70 ppm NO experiments are taken from [30].

The measured and simulated first-stage and main ignition delay times for different mixtures are summarized in Figs. 2 and 3, as functions of inverse temperature. As can be seen from Figs. 2 and 3, at both Pc = 20 and 40 bar, all the mixtures exhibit typical two-stage ignition behavior within the low-temperature regime, NTC (negative temperature coefficient) behavior, and typical single-stage ignition behavior within the intermediate to high temperature regimes. The largest effect is observed with only 70 ppm NO addition, where it promotes autoignition reactivity of PACE-20 at all temperatures and pressures. Olefin additions on top of 70 ppm NO have relatively smaller influence in comparison to 70 ppm NO, with olefin additions seemingly diminishing the promoting effect of NO, making the mixture less reactive. Overall, the influences of olefin addition on first-

stage ignition reactivity seems to be greater than those on main ignition reactivity. At the highest olefin addition, the promoting effect on first-stage ignition reactivity from adding 70 ppm NO can be completely neutralized or even reversed. These trends are mostly obvious with propene (Figs. 2b and 3b) and iso-butene (Figs. 2c and 3c). For instance, at Pc = 40 bar, iso-butene addition reduces first-stage ignition reactivity compared to the case with 20% EGR and 70 ppm NO, and with 3200 ppm iso-butene addition, the first-stage ignition delay time becomes longer than the baseline case with 20% EGR.

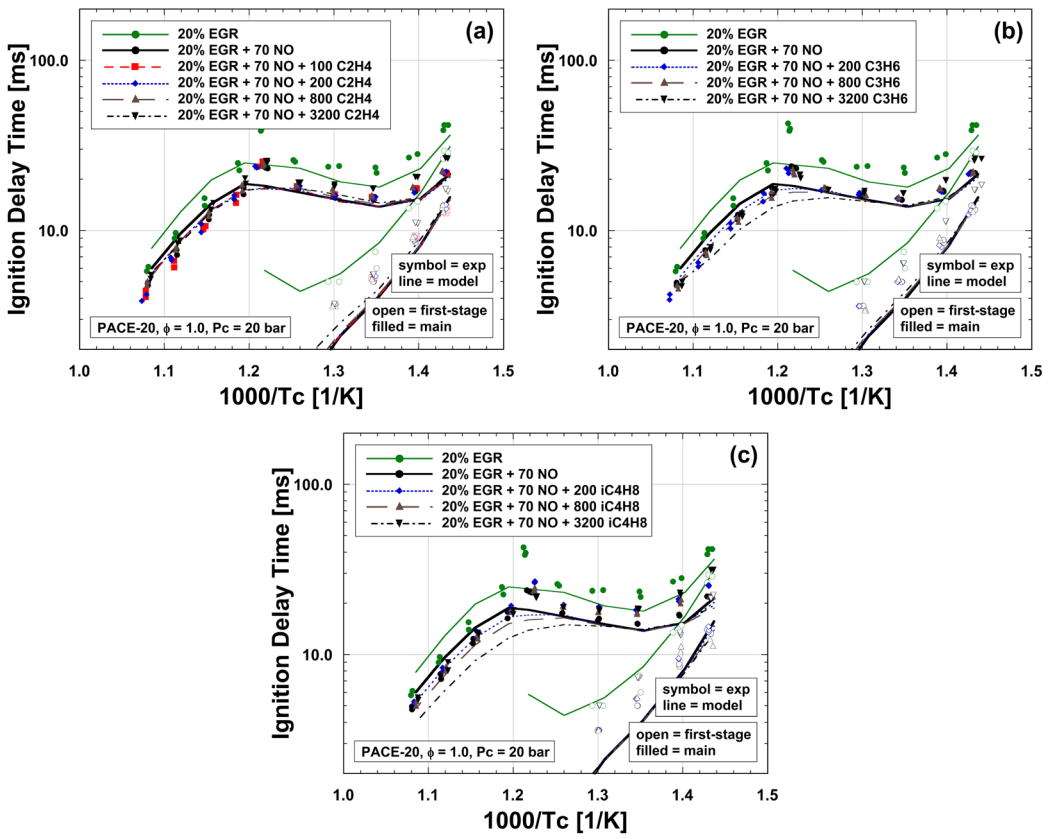

Figure 3. Measured (symbols) and simulated (lines) ignition delay times presented as functions of inverse temperature for PACE-20 with 20% EGR by mass, 70 ppm NO and different olefin concentrations (0, 100, 200, 800 and 3200 ppm) at **Pc = 20 bar**: (a) ethylene (C_2H_4); (b) propene (C_3H_6); (c) iso-butene (iC_4H_8). Lines – simulation results; symbols – experiments. 20% EGR + 70 ppm NO experiments are taken from [30].

Figure 4 presents the measured and simulated relative main ignition delay times for the PACE-20/20% EGR/70 ppm NO mixtures with four different levels of olefin addition (100 (only for

ethylene), 200, 800 and 3200 ppm) at Pc = 40 bar. The relative ignition delay time is used to better elucidate the perturbative effects of olefins on autoignition reactivity, which is defined as $\tau/\tau_{70ppmNO}$, where τ and $\tau_{70ppmNO}$ are the ignition delay times for the olefin-containing mixtures and the corresponding 0 ppm olefin case, respectively. It is important to recognize that although the overall measurement uncertainty (estimated at ±15% in Section 2.2.5) can be comparable to the variation in ignition delay times with small olefin additions at some conditions (e.g., 100 and 200 ppm at ~850 K in Fig. 4a), the trends at these small olefin addition levels are reproduced multiple times on different days to validate their fidelity.

At low temperatures (Tc < 800 K), all olefins tend to inhibit ignition reactivity, as shown in Fig. 4 where the relative ignition delay times become greater than 1.0 with olefin addition. The inhibiting effects of ethylene and propene are minor at low addition levels (e.g., 100 and 200 ppm), but become more pronounced at 800 ppm addition, and peak at 3200 ppm addition where ignition delay times are increased by 10–25%. The effects with iso-butene addition are considerably stronger than those with ethylene and propene. Specifically, 200 ppm iso-butene addition suppresses reactivity by ~20% (similar to the effects with 3200 ppm ethylene and propene), and 3200 ppm iso-butene further reduces the mixture reactivity to a level similar to the case without NO addition (i.e., the promoting effects from 70 ppm NO addition are nearly eliminated with 3200 ppm iC4H8 addition). The inhibiting effects of olefin at low temperatures could be due to the chemical kinetic interactions between the olefins and PACE-20 derivatives, or between the olefins and NO_x, or a combination of both.

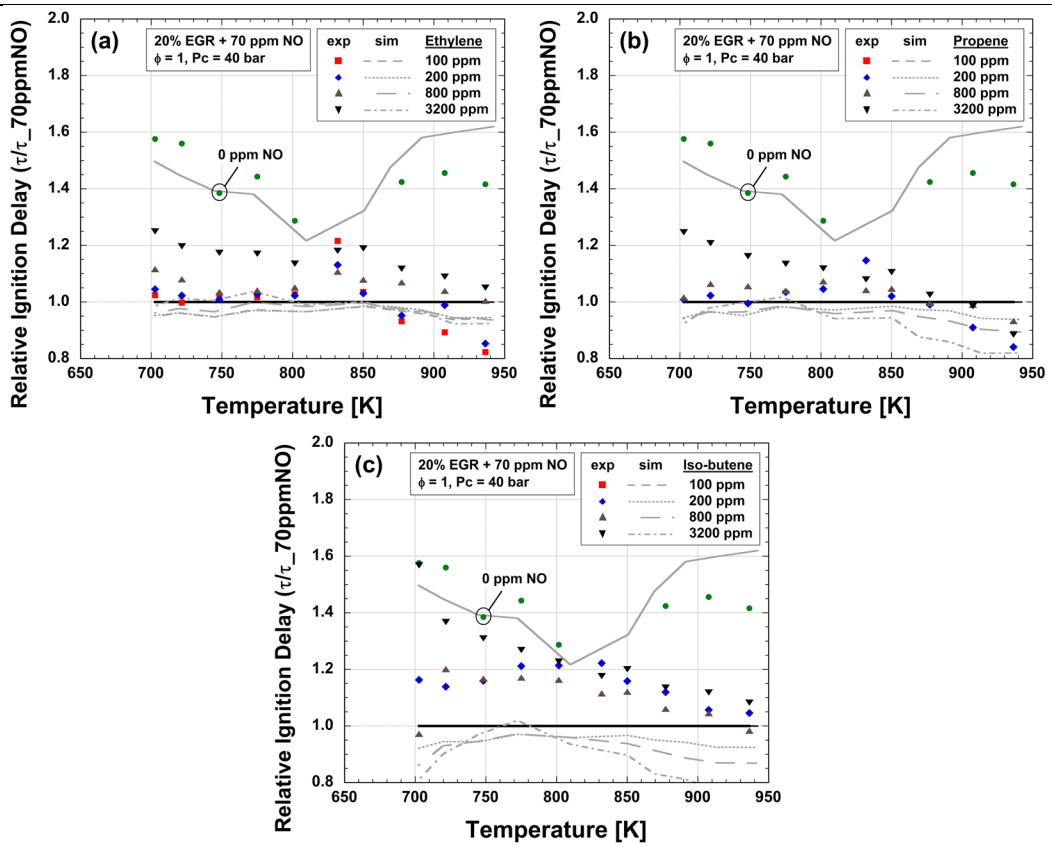

Figure 4. Measured (symbols) and simulated (lines) relative main ignition delay times for PACE-20 at ϕ = 1.0 and Pc = 40 bar with 20% EGR by mass, 70 ppm NO and different olefin concentrations: (a) ethylene (C_2H_4); (b) propene (C_3H_6); (c) iso-butene (iC_4H_8). The results without olefin and NO additions (green lines) are also included for comparison.

At intermediate temperatures (Tc > 850 K), ethylene and propene also display similar blending effects, with olefin addition ≤ 200 ppm promoting autoignition reactivity. However, at further olefin addition, the promoting effect is reversed and both olefins inhibit autoignition reactivity. This is most obvious for ethylene (Fig. 4a). For instance, at Tc = 900 K, 100 ppm ethylene addition reduces ignition delay time by 10%, whereas 800 and 3200 ppm ethylene additions increase ignition delay time by around 5% and 10%, respectively, indicating that there is a competing mechanism between the inhibiting and promoting chemical kinetic interactions from ethylene and propene addition. iso-Butene, on the other hand, does not display promoting effects, with all addition levels leading to a reduced autoignition reactivity.

To identify olefin addition effects on preliminary heat release characteristics, the LHV-normalized, experimental HRR for PACE-20 with 20% EGR, 70 ppm NO addition and different

olefin additions (0, 200, 800 and 3200 ppm) at Pc = 40 bar and Tc = 750 K are illustrated in Fig. 5 as functions of accumulated heat release. Figure 5 shows a typical two-stage hear release behavior for all the mixtures, where the first "bump" in the insets indicates the LTHR process. LTHR accounts for approximately 4% of the total LHV of the mixture for all cases. The effect of olefin addition is most pronounced on LTHR, less significant on HTHR and negligible on ITHR. Specifically, all olefins suppress the peak HRR during LTHR, with the suppressing effect following the order: iso-butene > ethylene > propene, which is consistent with the trends observed with first-stage ignition delay times in Fig. 2. iso-Butene addition also imposes the largest influence on HTHR, where ≤ 800 ppm addition suppresses the peak HRR during HTHR, while 3200 ppm addition promotes peak HRR.

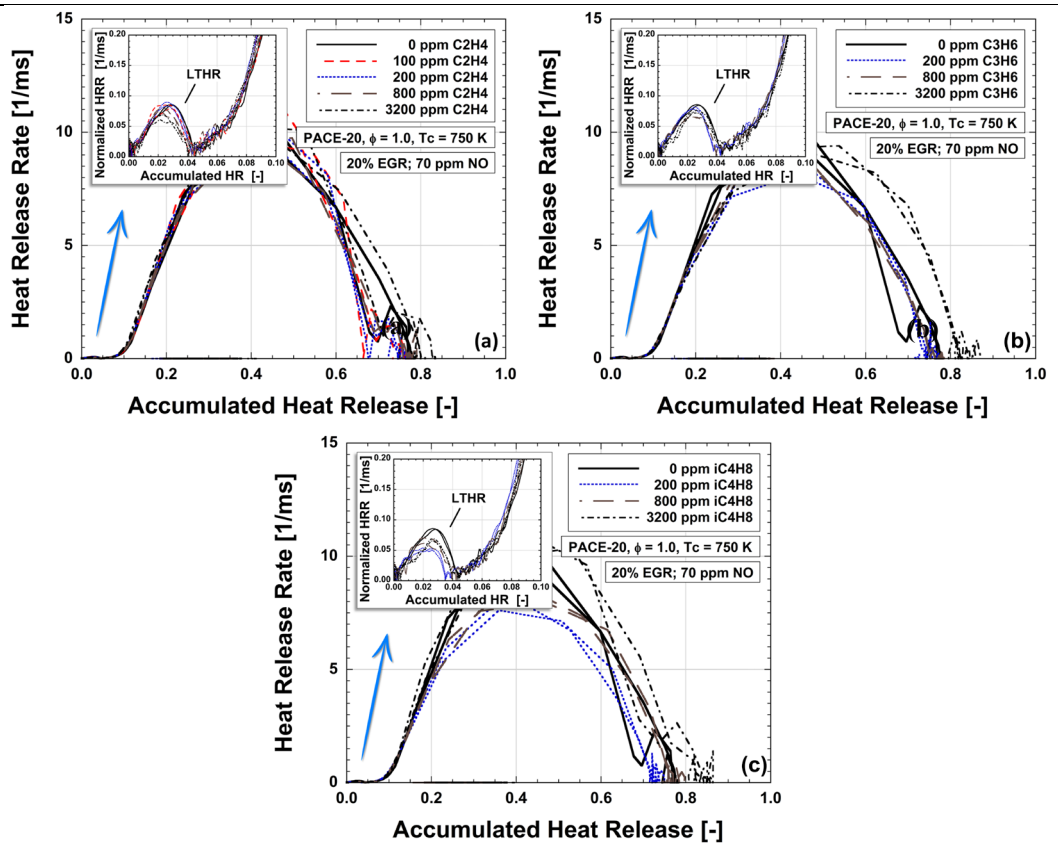

Figure 5. Calculated, normalized **experimental** heat release rates presented as functions of accumulated heat release for PACE-20 at phi = 1.0, Tc = 750 K and Pc = 40 bar with 20% EGR by mass, 70 ppm NO and different olefin concentrations: (a) ethylene (C_2H_4); (b) propene (C_3H_6); (c) iso-butene (iC_4H_8). Insets are used to highlight the changes in LTHR and ITHR

The performance of the chemical kinetic model in replicating the global trends of the RCM experiments can be also seen in Figs. 2 and 3, where the model captures the two-stage ignition behavior at low temperatures, as well as the typical NTC and Arrhenius behaviors at NTC-to-intermediate temperatures at both Pc = 20 and 40 bar. For first-stage ignition reactivity, the model shows excellent agreement for the baseline case with 0 ppm NO and 0 ppm olefin, while consistently overpredicting reactivity with 70 ppm NO at all olefin concentrations. Despite the quantitative discrepancy, the model captures the inhibiting effects of all olefins on first-stage ignition reactivity, particularly at 3200 ppm olefin addition. On the other hand, the inadequate model performance in replicating the quantitative olefin addition effects can be better seen in Fig. 4. Comparing the modeling results across different olefins, the model captures the greater perturbative effects from iso-butene addition than ethylene and propene additions. Nevertheless, the model indicates that all olefins promote main ignition reactivity, while experimental promoting effects are only observed for ethylene and propene addition at Tc > 850 K. Further improvement of the chemical kinetic model is needed to achieve better quantitative agreement with the experimental olefin addition effects.

3.2 Sensitivity and rate of production (ROP) analysis

To provide understandings of the interactive chemistry between EGR olefins and PACE-20/NO, and draw necessary insight to guide future efforts to improve the chemical kinetic model, sensitivity and ROP analyses are conducted.

Brute force sensitivity analysis on main ignition delay time is first conducted for 0 and 800 ppm olefin mixtures at Pc = 40 bar and Tc = 750 and 900 K. The sensitivity coefficients are defined as $S_{rel} = \ln\left(\frac{\tau^{\Delta}}{\tau}\right) / \ln\left(\frac{k^{\Delta}}{k}\right)$, where τ^{Δ} and τ are the ignition delay times after multiplying and dividing, respectively, the original rate constant by 2. Negative sensitivity coefficients indicate that the reaction promotes reactivity, while positive coefficients indicate an inhibiting effect. Figure 6 presents the computed sensitivity coefficients for the top sensitive reactions, where the participating species can be identified in the species dictionary in the Supplementary Material.

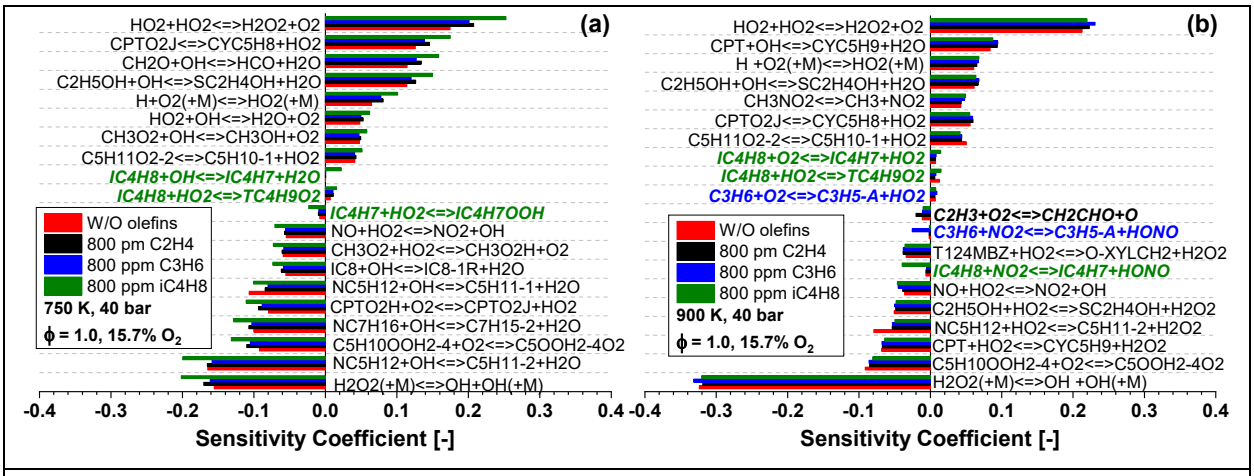

Figure 6. Sensitivity analysis on main ignition delay times for PACE-20 at ϕ = 1.0 and Pc = 40 bar with 20% EGR by mass, 70 ppm NO and different olefin concentrations: (a) Tc = 750 K; (b) Tc = 900 K. Olefin interacting pathways are highlighted in ***italic***.

At Tc = 750 K (Fig. 6a), adding 800 ppm ethylene or propene does not lead to significant changes in the sensitivity for the most sensitive reactions. This is somewhat consistent with the modeling results in Fig. 4, where the impact of 800 ppm ethylene or propene addition on main ignition reactivity is relatively minor. However, with 800 ppm iso-butene addition, there is a clear shift in the most sensitive reactions toward iso-butene chemistry. There is distinct growth in the sensitivity of OH- and HO_2-consuming pathways from iso-butene chemistry, via $iC_4H_8+OH \leftrightarrow iC_4H_7+H_2O$ and $iC_4H_7+HO_2 \leftrightarrow iC_4H_7OOH$, respectively. The former suppresses reactivity due to the consumption of OH radicals, while the latter promotes reactivity as iC_4H_7OOH subsequently leads to OH formation.

At Tc = 900 K (Fig. 6b), the interaction between olefins and other sub-mechanisms becomes even stronger, compared to that at Tc = 750 K. For propene and iso-butene, there are two types of interaction among the most sensitive reactions, i.e., the interactions between the olefins and NO_x species such as the H-abstractions by NO_2 from olefins that promote reactivity, and the interactions such as chain-terminations between HO_2 radicals and olefinic resonantly-stabilized radicals that form olefin + O_2 that inhibit reactivity. With 800 ppm iso-butene or propene addition, the sensitivity for the promoting olefin+NO_2 pathways increases greatly, while those for the inhibiting olefin+O_2 pathways remain similar to the baseline (i.e., the case without olefin addition). This aligns well with the simulation results in Fig. 4b and 4c, where main ignition reactivity is greatly enhanced with 800 ppm propene and iso-butene. The contribution to the most sensitive reactions

by 800 ppm ethylene addition is less significant than propene and iso-butene, which is, again, consistent with the simulation results in Fig. 4.

ROP analysis is carried out at 2% n-heptane consumption for the 0 and 800 ppm olefin addition cases at the same conditions as in Fig. 6. 2% n-heptane consumption is selected to track olefin interacting pathways at the start of the oxidation process. All olefins, including ethylene, propene and iso-butene, as well as their primary products (e.g., C_2H_3, C_3H_5-A and iC_4H_7, respectively) are included in the analysis. The results covering the most dominant pathways are presented in Fig. 7.

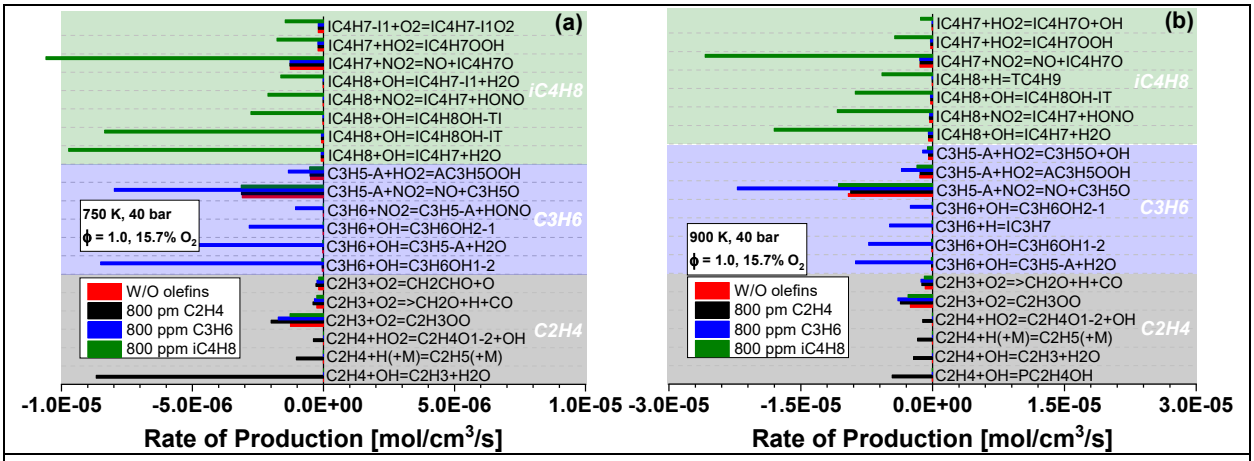

Figure 7. ROP analysis of olefins and their primary derivatives for PACE-20 at ϕ = 1.0 and Pc = 40 bar with 20% EGR by mass, 70 ppm NO and different olefin concentrations: (a) Tc = 750 K; (b) Tc = 900 K.

At both Tc = 750 and 900 K, adding olefins leads to considerably increased flux of the consuming pathways for all three olefins, as well as their primary derivatives except for C_2H_3, with greater increment observed at Tc = 900 K. The increase in flux for the olefin consuming pathways is most distinct, in comparison to the baseline case (i.e., without olefin addition) where the flux of these pathways is negligible.

For iso-butene, there is a competing mechanism between the iso-butene consuming pathways from different sub-chemistries at both Tc = 750 and 900 K, where the added iso-butene can interact with OH to form iC_4H_7 and iC_4H_8OH, or directly with NO_2 via $iC_4H_8+NO_2 \leftrightarrow iC_4H_7+HONO$. Though iso-butene/$NO_x$ interactions are less dominant among the iso-butene consuming pathways, their contribution to iC_4H_7 consumption via $iC_4H_7+NO_2 \leftrightarrow NO+iC_4H_7O$ is overriding. Despite the inhibiting effect from $iC_4H_8+OH \leftrightarrow iC_4H_7+H_2O$ shown in Fig. 6a, the overall autoignition reactivity

is still promoted (c.f., Fig. 4c) via $iC_4H_8+NO_2\leftrightarrow iC_4H_7+HONO$ and $iC_4H_7+NO_2\leftrightarrow NO+iC_4H_7O$ since they lead to the formation of NO that greatly facilitate OH production via $NO+HO_2\leftrightarrow NO_2+OH$ [15]. It might be somewhat counter-intuitive that iso-butene/NO_2 interactions pathways are quite important at this stage, given that NO_2 does not exist in the initial mixture. Although the initial mixture does not contain NO_2, NO_2 can be produced rapidly via $NO+ROO=NO_2+RO$ and $NO+HO_2=NO_2+OH$ during the initial oxidation process, as concluded in [30].

The same competing mechanism is also observed for propene, where propene can be consumed via OH participating pathways that lead to the formation of either C_3H_5-A or C_3H_6OH, or via direct interaction with NO_2 that leads to NO production. Propene/NO_x interaction is also the main contributor to C_3H_5-A consumption, with $C_3H_5\text{-A}+NO_2\leftrightarrow NO+C_3H_5O$ accounting for over 70% of total C_3H_5-A consumption at this stage. The promoting effect of propene addition on autoignition reactivity in the simulation results can also be attributed to these propene/NO_x interactions that facilitate NO production.

The influence of 800 ppm ethylene addition is the smallest among the three olefins. This is consistent with the simulation results in Fig. 4, where ethylene imposes the smallest change to main ignition reactivity. Major contributors to the consumption of ethylene are H-abstraction reaction by OH and OH addition reaction that form C_2H_3 and PC_2H_4OH, respectively. C_2H_3 can react with molecular O_2 to promote reactivity (Fig. 6b), and PC_2H_4OH undergoes the Waddington Mechanism that results in a net-zero OH production [28].

4. Conclusion

The role of EGR olefins (namely ethylene, propene and iso-butene) in perturbing gasoline autoignition and heat release characteristics with the presence of 70 ppm NO is investigated in ANL's tpRCM at five different olefin concentrations (0, 100, 200, 800 and 3200 ppm) under a stoichiometric fuel loading with 20% EGR by mass, pressures of 20 and 40 bar, and temperatures from 680 to 950 K.

RCM measurements show that at Tc < 850 K, all EGR olefins inhibit autoignition reactivity and LTHR, with iso-butene exhibiting the greatest impact among the three olefins, while at Tc >850 K, ethylene and propene can promote reactivity. The chemistry model captures the inhibiting effects of all olefins on first-stage ignition reactivity, while consistently predicting a promoting

effect on main ignition reactivity, which is inconsistent with the experiments. Sensitivity and ROP analyses indicate that added olefins greatly alter the role of consuming pathways for olefins and their primary derivatives at the initial stage of oxidation process, and reveal that there is a competing mechanism between these consuming pathways, where olefin addition can lead to OH scavenging, propagation and branching via H-abstraction by OH, OH addition and interactions with NO_2, respectively. The olefin/NO_x interactions are particularly pronounced with propene and iso-butene addition and are most likely responsible for the discrepancies between the model and experiments.

Through both experimental and numerical frameworks, this study unravels the role and highlights the importance of EGR olefins, particularly in the presence of NO, in gasoline combustion at engine representative conditions, which has been overlooked in the past. Disagreements between model predictions and experimental measurements require further investigation of olefin interacting chemistry, particularly those with NO_x.

Acknowledgement

The work at ANL and LLNL were supported by the U.S. Department of Energy PACE Initiative with Gurpreet Singh and Michael Weismiller as program managers, under contract No. DE-AC02-06CH11357 and DE-AC52-07NA27344, respectively. The work at The Hong Kong Polytechnic University were supported by the University Grant Council under projects P0039589 and P0043026.

Supplementary material

SMM1 includes uncertainty analysis on olefin concentrations in the mixtures; SMM2 lists the species identifiers; SMM3 include the summary of experimental results; and SMM4 includes the volume-time histories derived from non-reactive tests.

References

[1] H. Wei, T. Zhu, G. Shu, L. Tan, Y. Wang, Gasoline engine exhaust gas recirculation – A review, Appl. Energ. 99 (2012) 534-544.

[2] M. Yao, Z. Zheng, H. Liu, Progress and recent trends in homogeneous charge compression ignition (HCCI) engines, Prog. Energy Combust. Sci. 35 (2009) 398-437.

[3] T. Alger, B. Mangold, C. Roberts, J. Gingrich, The Interaction of Fuel Anti-Knock Index and Cooled EGR on Engine Performance and Efficiency, SAE Int. J. Engines 5 (2012) 1229-1241.

[4] J.P. Szybist, S.W. Wagnon, D. Splitter, W.J. Pitz, M. Mehl, The Reduced Effectiveness of EGR to Mitigate Knock at High Loads in Boosted SI Engines, SAE Int. J. Engines 10 (2017) 2305-2318.

[5] M. Koegl, B. Hofbeck, S. Will, L. Zigan, Influence of EGR and ethanol blending on soot formation in a DISI engine, Proc. Combust. Inst. 37 (2019) 4965-4972.

[6] M. Sjöberg, J.E. Dec, Effects of EGR and its constituents on HCCI autoignition of ethanol, Proc. Combust. Inst. 33 (2011) 3031-3038.

[7] W. Zeng, M. Sjöberg, D.L. Reuss, Combined effects of flow/spray interactions and EGR on combustion variability for a stratified DISI engine, Proc. Combust. Inst. 35 (2015) 2907-2914.

[8] B.M. Gauthier, D.F. Davidson, R.K. Hanson, Shock tube determination of ignition delay times in full-blend and surrogate fuel mixtures, Combust. Flame 139 (2004) 300-311.

[9] A. Vandersickel, M. Hartmann, K. Vogel, Y.M. Wright, M. Fikri, R. Starke, C. Schulz, K. Boulouchos, The autoignition of practical fuels at HCCI conditions: High-pressure shock tube experiments and phenomenological modeling, Fuel 93 (2012) 492-501.

[10] H. Li, L. Yu, S. Sun, S. Wang, X. Lu, Z. Huang, A Shock Tube Experimental and Modeling Study of Multicomponent Gasoline Surrogates Diluted with Exhaust Gas Recirculation, Energy Fuels 32 (2018) 3800-3813.

[11] L. Cai, A. Ramalingam, H. Minwegen, K. Alexander Heufer, H. Pitsch, Impact of exhaust gas recirculation on ignition delay times of gasoline fuel: An experimental and modeling study, Proc. Combust. Inst. 37 (2019) 639-647.

[12] Y. Song, Y. He, Y. Yu, B. Moreau, F. Foucher, Effect of Exhaust Gas Recirculation and NO on Ignition Delay Times of Iso-octane in a Rapid Compression Machine, Energy Fuels 34 (2020) 8788-8795.

[13] S. Cheng, C. Saggese, D. Kang, S.S. Goldsborough, S.W. Wagnon, G. Kukkadapu, K. Zhang, M. Mehl, W.J. Pitz, Autoignition and preliminary heat release of gasoline surrogates and their blends with ethanol at engine-relevant conditions: Experiments and comprehensive kinetic modeling, Combust. Flame 228 (2021) 57-77.

[14] S. Cheng, D. Kang, A. Fridlyand, S.S. Goldsborough, C. Saggese, S. Wagnon, M.J. McNenly, M. Mehl, W.J. Pitz, D. Vuilleumier, Autoignition behavior of gasoline/ethanol blends at engine-relevant conditions, Combust. Flame 216 (2020) 369-384.

[15] R. Fang, C. Saggese, S.W. Wagnon, A.B. Sahu, H.J. Curran, W.J. Pitz, C.-J. Sung, Effect of nitric oxide and exhaust gases on gasoline surrogate autoignition: iso-octane experiments and modeling, Combust. Flame 236 (2022) 111807.

[16] J. Szybist, Knock Mitigation Effectiveness of EGR across the Pressure-Temperature Domain, SAE Int. J. Adv. Curr. Pract. Mobil. 3 (2020) 262-275.

[17] Y. Kobashi, M. Todokoro, G. Shibata, H. Ogawa, T. Mori, D. Imai, EGR gas composition effects on ignition delays in diesel combustion, Fuel 281 (2020) 118730.

[18] F. Zhang, H.-y. Chen, J.-c. Feng, D. Zheng, Experimental investigation of auto-ignition of ethylene-nitrous oxide propellants in rapid compression machine, Fuel 288 (2021) 119688.

[19] A. Ramalingam, S. Panigrahy, Y. Fenard, H. Curran, K.A. Heufer, A chemical kinetic perspective on the low-temperature oxidation of propane/propene mixtures through experiments and kinetic analyses, Combust. Flame 223 (2021) 361-375.

[20] C.-W. Zhou, Y. Li, E. O'Connor, K.P. Somers, S. Thion, C. Keesee, O. Mathieu, E.L. Petersen, T.A. DeVerter, M.A. Oehlschlaeger, G. Kukkadapu, C.-J. Sung, M. Alrefae, F. Khaled, A. Farooq, P. Dirrenberger, P.-A. Glaude, F. Battin-Leclerc, J. Santner, Y. Ju, T. Held, F.M. Haas, F.L. Dryer, H.J. Curran, A comprehensive experimental and modeling study of isobutene oxidation, Combust. Flame 167 (2016) 353-379.

[21] S. Cheng, S.S. Goldsborough, S.W. Wagnon, R. Whitesides, M. McNenly, W.J. Pitz, D. Lopez-Pintor, J.E. Dec, Replicating HCCI-like autoignition behavior: what gasoline surrogate fidelity is needed?, App. Energy Combust. Sci. 2022 (under review).

[22] A. Fridlyand, S.S. Goldsborough, M. Al Rashidi, S.M. Sarathy, M. Mehl, W.J. Pitz, Low temperature autoignition of 5-membered ring naphthenes: Effects of substitution, Combust. Flame 200 (2019) 387-404.

[23] T. Rockstroh, A. Fridlyand, S. Ciatti, W. Cannella, S.S. Goldsborough, Autoignition behavior of a full boiling-range gasoline: Observations in RCM and GCI engine environments, Combust. Flame 209 (2019) 239-255.

[24] M. Sjöberg, J.E. Dec, W. Hwang, Thermodynamic and Chemical Effects of EGR and Its Constituents on HCCI Autoignition, SAE Trans. 116 (2007) 271-289.

[25] A. Dubreuil, F. Foucher, C. Mounaim-Rousselle, Effect of Chemical Components, Amount and Temperature of the Exhaust-Gas-Recirculation on the Combustion Development in HCCI Mode, Proc. THIESEL, (2006) 629-631.

[26] J.B. Heywood, Internal combustion engine fundamentals, McGraw-Hill, New York, 1988.

[27] S. Cheng, S.S. Goldsborough, S.W. Wagnon, W.J. Pitz, Probing intermediate temperature heat release in autoignition of C3-C4 iso-alcohol/gasoline blends, Combust. Flame 233 (2021) 111602.

[28] S. Cheng, D. Kang, S.S. Goldsborough, C. Saggese, S. Wagnon, W.J. Pitz, Experimental and modeling study of C2-C4 alcohol autoignition at intermediate temperature conditions, Proc. Combust. Inst. 38 (2021) 709-717.

[29] S. Cheng, Y. Yang, M.J. Brear, M. Frenklach, Quantifying uncertainty in kinetic simulation of engine autoignition, Combust. Flame 216 (2020) 174-184.

[30] S. Cheng, C. Saggese, S.S. Goldsborough, S.W. Wagnon, W.J. Pitz, Chemical kinetic interactions of NO with a multicomponent gasoline surrogate: experiments and modeling, Proc. Combust. Inst. 2023 (under review).

[31] W.-T. Chan, S.M. Heck, H.O. Pritchard, Reaction of nitrogen dioxide with hydrocarbons and its influence on spontaneous ignition. A computational study, Phys. Chem. Chem. Phys. 3 (2001) 56-62.

[32] Y. Choi, M.-C. Lin, Kinetics and mechanisms for reactions of HNO with CH3 and C6H5 studied by quantum‐chemical and statistical‐theory calculations, Int. J. Chem. Kinet. 37 (2005) 261-274.

[33] J.A. Miller, C.T. Bowman, Mechanism and modeling of nitrogen chemistry in combustion, Prog. Energy Combust. Sci. 15 (1989) 287-338.

[34] D. Liu, B.R. Giri, M. Szőri, B. Viskolcz, E.-t. Es-sebbar, A. Farooq, On the redox reactions between allyl radicals and NOx, Proc. Combust. Inst. 38 (2021) 967-976.

[35] P. Gokulakrishnan, C.C. Fuller, M.S. Klassen, Experimental and modeling study of C1–C3 hydrocarbon ignition in the presence of nitric oxide, J. Eng. Gas Turbines Power 140 (2018).

[36] C.A. Almodovar, C.F. Goldsmith, Laser schlieren study of the thermal decomposition of 2-ethylhexyl-nitrate, Proc. Combust. Inst. 38 (2021) 997-1005.

[37] R. Atkinson, D. Baulch, R. Cox, J. Crowley, R. Hampson, R. Hynes, M. Jenkin, M. Rossi, J. Troe, I. Subcommittee, Evaluated kinetic and photochemical data for atmospheric chemistry: Volume II–gas phase reactions of organic species, Atmos. Chem. Phys. 6 (2006) 3625-4055.

[38] M.J. McNenly, R.A. Whitesides, D.L. Flowers, Faster solvers for large kinetic mechanisms using adaptive preconditioners, Proc. Combust. Inst. 35 (2015) 581-587.